Materials Research Bulletin 60 (2014) 88–96

Contents lists available at ScienceDirect

Materials Research Bulletin

journal homepage: www.elsevier.com/locate/matresbu

Renewable energy in focus: In_5Se_5Br, a solid material with promising thermoelectric properties for industrial applications

Kledi Xhaxhiu [a,*], Carita Kvarnström [b], Pia Damlin [b], Klaus Bente [c]

[a] Department of Chemistry, Faculty of Natural Sciences, University of Tirana, 1001 Tirana,Albania
[b] Department of Chemistry, Faculty of Mathematics and Natural Sciences, University of Turku, Vatselankatu 2, 20014 Turku, Finland
[c] Institute of Mineralogy, Crystallography and Materials Science, Faculty of Chemistry and Mineralogy, University of Leipzig, Scharnhorststraße 20, 04275 Leipzig, Germany

ARTICLE INFO

Article history:
Received 6 January 2014
Received in revised form 10 July 2014
Accepted 4 August 2014
Available online 7 August 2014

Keywords:
Mixed valence chalcogenid halides
n-type semiconductor
Solid state synthesis
High temperature-XRD
Thermoelectric
Photoelectric

ABSTRACT

We obtained via solid state synthesis needle-shaped crystals of In_5Se_5Br crystallizing in the space group $Pmn2_1$ and containing indium simultaneously in three different oxidation states: In^+, formal In^{2+} and In^{3+}. Bulk sample of In_5Se_5Br shows *n*-type conductivity and linear increase of Seebeck voltage with the temperature difference increase. Seebeck voltage of approx. 720 mV is recorded at a temperature difference of 80 K, corresponding to a Seebeck coefficient −8900 μV/K. A voltage increase up to 250 mV is recorded within 10 min upon application of a 27 K temperature difference between the contacts. On-off switching of the heating source unveils repeatable results. Linear *I–U* behavior with a resistivity of $2.32 \times 10^{11}\ \Omega$ is observable for individual needles of In_5Se_5Br. In bulk In_5Se_5Br the resistivity oscillates between 2.6 MΩ and 23 MΩ. DTA and HT-powder XRD data show incongruent melting to InBr, InSe and In_2Se_3 at 805 K. The ternary compound expands 1.02% along [0 1 0] showing a coefficient of thermal expansion $\alpha_b = 2.3(4) \times 10^{-5}\ K^{-1}$. Lower expansions of 0.6% and 0.16% along *a* and *c* axes corresponding to mean coefficients of thermal expansion of $\overline{\alpha_a} = 1.3(1) \times 10^{-5}\ K^{-1}$, $\overline{\alpha_c} = 4.4(5) \times 10^{-6}\ K^{-1}$ are observed. Thin layer growing of In_5Se_5Br on glass substrate with targeted doping/substitutions can improve the sample conductivity, increase the Seebeck coefficient and lower the thermal conductivity making In_5Se_5Br a good alternative material for industrial thermoelectric applications.

1. Introduction

Thermoelectrics are materials that are able to convert thermal energy, considered often as the "lost energy" into electricity and vice versa. They are used for power generation utilizing the Seebeck effect for heat pumping and refrigeration (Peltier effect). The applicability of these devices is mostly limited due to their low efficiency. A good thermoelectric material (TE) should have large Seebeck coefficient (S), high electrical conductivity (σ) and low thermal conductivity (κ) [1]. In order to get a high efficiency, the dimensionless thermoelectric figure-of-merit ZT defined as: $ZT = (S^2\sigma/\kappa)$ should be >1. Therefore the challenge in this filed remains in the optimization of the transport properties by synthesizing materials with high S and σ and low lattice thermal conductivity. Materials that best meet these requirements are typically heavily doped, small band gap semiconductors or semimetals. Such materials provide a balance between the high Seebeck coefficient of semiconductors and the low electrical resistivity of metals. Si–Ge alloys [2], transition-metal disilicides [3–5], metal chalcogenides [6,7], several boron compounds [8,9], and the oxide material $TiO_{1.1}$ [10] have attracted attention for high-temperature thermoelectric applications, where the lattice contribution is less important. Several promising classes of new materials have been identified including the binary compounds Sb_2Ch_3 and Bi_2Ch_3 (Ch = S, Se, Te) and their mixed crystals [11–16], tetradymides and tetradymide-like compounds [17–21], scutterudites and scutterudite-like compounds [22–29], clathrates [30–33] and half-Heusler alloys [34,35]. $CsBi_4Te_6$ was recently reported as a high-performance thermoelectric material with a maximum ZT ~0.8 at 225 K [36]. $AgPb_mSbTe_{2+m}$ with common structural features and similar lattice thermal conductivities as Bi_2Te_3 shows a spectacular thermoelectric figure of merit ($ZT > 2$) [37–39]. Beside all these mentioned materials with pronounced thermoelectric behavior, there is a great number of natural and synthetic sulfosalts showing promising thermoelectric properties [40–45]. Boulangerite ($Pb_{5\pm x}Sb_{4\pm x}S_{11\pm 1/2x}$) and cylindrite ($Fe_{1\pm m}Sn_{4\pm x}Pb_{3\pm y}Sb_{2\pm z}S_{14}$) are quite appealing sulfosalts obtained by chemical vapor transport crystallizing as micro- and

* Corresponding author.
E-mail address: kledi.xhaxhiu@unitir.edu.al (K. Xhaxhiu).

http://dx.doi.org/10.1016/j.materresbull.2014.08.001
0025-5408/

nano-needles or cylinders exhibiting high Seebeck coefficient (−900 μV/K) [46]. Many other compounds of interest for this application have been already reported [47–49]. In the course of enriching the spectrum with efficient thermoelectric compounds, the goal o this study focuses on an alternative mixed valence chalcogenide–halide of indium with unusual high Seebeck coefficient and interesting electrical and thermal properties.

2. Experimental

2.1. Synthesis

The needle-shaped single crystals of In_5Se_5Br were prepared via solid state methods by annealing at 773 K for two weeks the stoichiometric mixtures of the elements In (tear drop 99.999%, Chempur, Karlsruhe, Germany), Se (shot 1–3 mm, 99.995%, Fluka, Buchs, Switzerland) and the binary compound $InBr_3$ (powder, 99.99%, Heraeus, Hanau, Germany) in evacuated quartz ampoules [50]. Bigger crystals were grown by the implementation of a slow temperature program, i.e., with low temperature increment (2 K/h). The samples were annealed for two weeks at 773 K and then slowly cooled down with a temperature decreasing rate of 5 K/h until 323 K.

2.2. TEM and EDX analyses

The surface morphology and bulk composition of the crystals were investigated by Electron Probe Micro-Analysis (EPMA) using a CAMECA SX-100 (CAMECA GmbH, Unterschleissheim/Munich, Germany) and by energy-dispersive X-ray (EDX) analysis using a JEOL 6400 SEM apparatus, equipped with a Robinson BSE (back scattering electron) and SE (secondary electron) detector.

2.3. Thermal analysis

The differential thermal analysis (DTA) suitable for qualitative investigations of phase transitions and melting behaviors of solids were performed in a "Linseis" device (Type: DTA L-62), Linseis Messgeraete GmbH, Selb, Germany. The sample and the reference (Al_2O_3) were enclosed in preheated evacuated and sealed quartz ampoules of 5 mm outer diameter and 10–20 mm length. The ampoules were placed into ceramic crucibles which were fixed on thermocouples. The samples were heated up to 700 °C and cooled down to 50 °C using a heating and cooling rate of 5 °C/min. The recorded temperature difference between the compound and the reference presented as a peak was evaluated using the delivered Linseis software package. The device calibration was performed using the elements Sn, Zn and Ag in the region of 232–962 °C.

2.4. X-ray powder investigations

Powder X-ray measurements for the characterisation of crystalline samples were performed with a powder diffraction device D5000 delivered by SIEMENS company (XRD; Siemens D5000, Bruker-AXS, Karlsruhe, Germany) using Cu $K\alpha_1$-radiation (λ = 1.54051 Å) in transmission mode. For the measurements, 50–100 mg of fine powdered sample was spread on a Mylar-foil (covered with a thin layer of silicon grease) and the foil was fixed on a flatbed holder. The diffraction patterns were recorded by means of a "Braun" position sensitive detector (PSD-50M) with an angular increment of 0.015° and a measuring time varying from 0.5–10 h. The indexation of the reflections and their refinements were performed by the X-Ray data software package VISUAL X^{POW} and WIN X^{POW} delivered from the "STOE" company, Darmstadt, Germany.

The X-ray temperature dependent measurements of powder samples were performed on a "STOE" transmission diffraction system type (STADI-P) using Cu-$K\alpha_1$-radiation. The onset temperature calibration occurred using an iridium standard (a = 3.8388 Å). The determination of the reflection positions of the iridium sample was performed through peak-profile fitting using Lorentzian function.

2.5. Thermoelectric (Seebeck voltage) measurements

A self made device was used for the determination of Seebeck coefficient of all compounds. It consisted of a Bakelite body in which two arrow-shaped metallic contacts were installed (Fig. 1a).

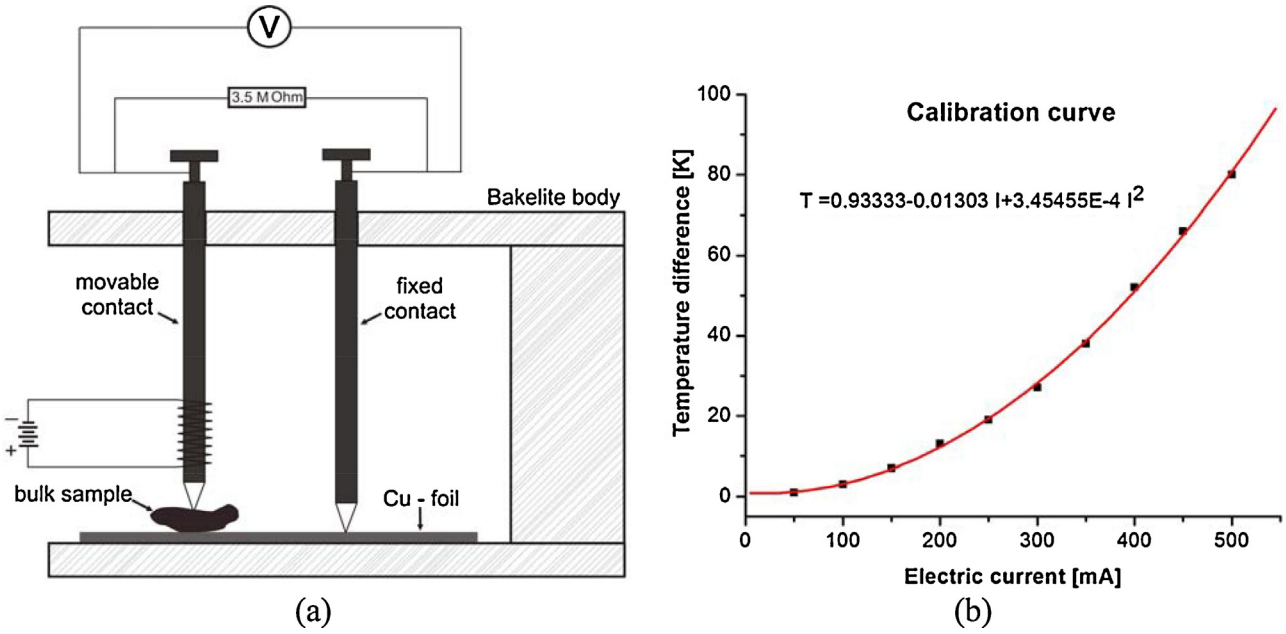

Fig. 1. (a) Scematic of a self made device for thermoelectric measurements of thin films and solid bulk samples, (b) the calibration curve as a plot of temperature difference between both contacts and the electric current applied.

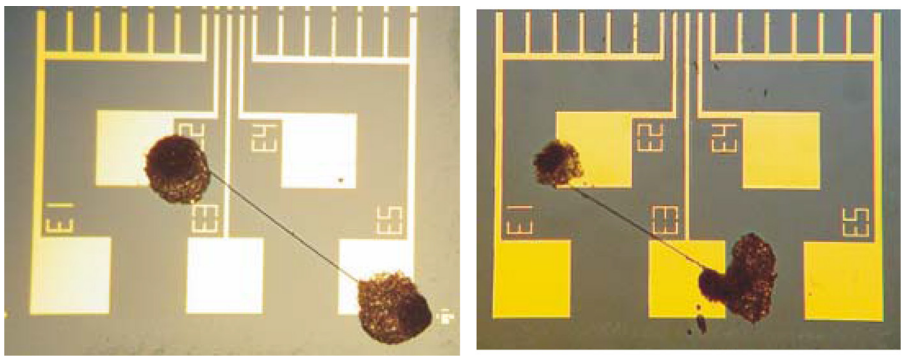

Fig. 2. Optical-microscope assisted pictures of needle-shaped crystals contacted on prefabricated micro-chips with golden structure employed for the determination of electric conductivity of microwires.

Both contacts were joined by a shunt resistor of 3.5 MΩ and further connected to a precise voltage meter. The movable contact (bulk sample-shape adjustable), was equipped with an electric heating coil close to its bottom tip. The electric heating coil was controlled by an external electric power unit. The hot contact spikes the sample surface, while the fixed one spikes the copper foil, serving as electricity conductor. The temperature difference variation between both contacts plotted against the applied electric current of the hot contact served as the device's calibration curve (Fig. 1b).

The temperature of the movable contact was adjusted through the variation of the electric current flowing to the heating coil. This was done by means of a power generator VOLTCRAFT PLUS VSP 1410HE. The temperature difference between the hot and cold contacts was measured using an in-situ coupled thermoelement controlled by a KEITHLEY 175 AUTORANGING MULTIMETER.

During the measurement, the single crystal, film or bulk sample was tipped from both contacts if long enough or tipped by one contact while the other contacts a cooper foil laying underneath the sample. In this case, the cooper foil plays the role of the charge conductor. All the measurements were performed in dark due to the light-dependent conductivity of In_5Se_5Br.

2.6. Conductivity measurements (I–U curves)

Electrical measurements of single needle shaped crystals were performed at room temperature using pre-fabricated micro chips with golden structure. The individual needles were carefully selected by means of an optical microscope and were carefully placed between two electrodes of a chip. Both ends of the individual needle were contacted to the microchip electrodes using silver contacting epoxy (Fig. 2). The as prepared microchips with the dimensions 3 mm × 4 mm were thermally treated in a thermostat at 70 °C for 2 h. The *I–U* curves of the individual needles and bulk sample were measured in dark within an Agilent 4155C Semiconductor Parameter Analyser, Waldbronn, Karlsruhe, Germany.

3. Discussion of the results

3.1. Crystal's morphology and content

The solid material obtained from the above described synthesis consisted of fine dark-brownish needle-shaped crystals with

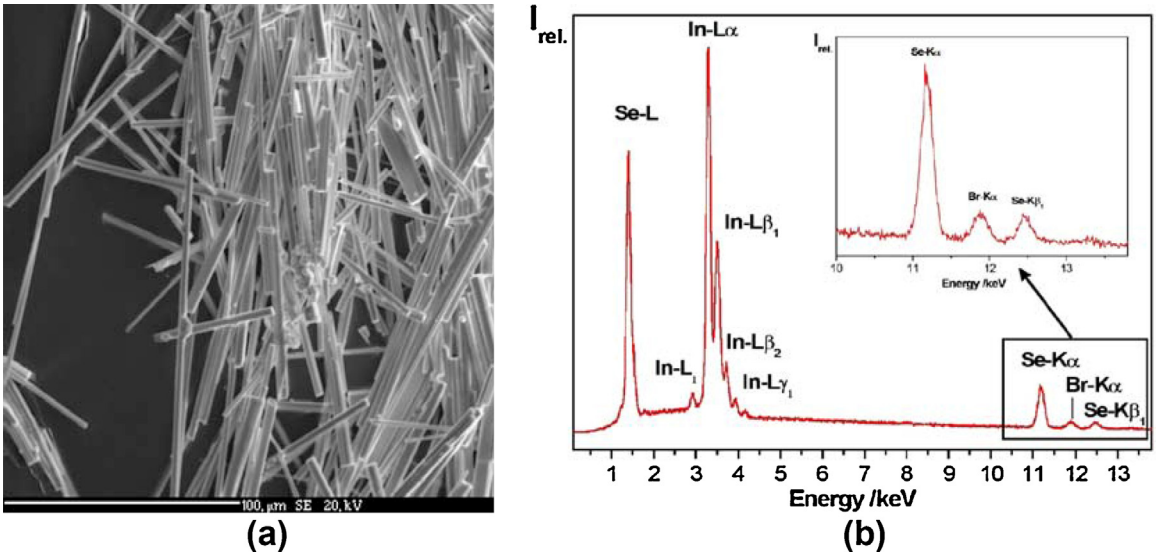

Fig. 3. (a) TEM image of nano- and micro crystals of In5Se5Br, (b) EDX spectrum of the dark-brown needle-shaped crystals of In_5Se_5Br, for a better visualisation the section from 11.5–14 keV is magnified. The Br-L line overlaps with the Se-L line, the presence of bromine is confirmed by the Br-Kα line. (For interpretation of the references to colour in this figure legend, the reader is referred to the web version of this article.)

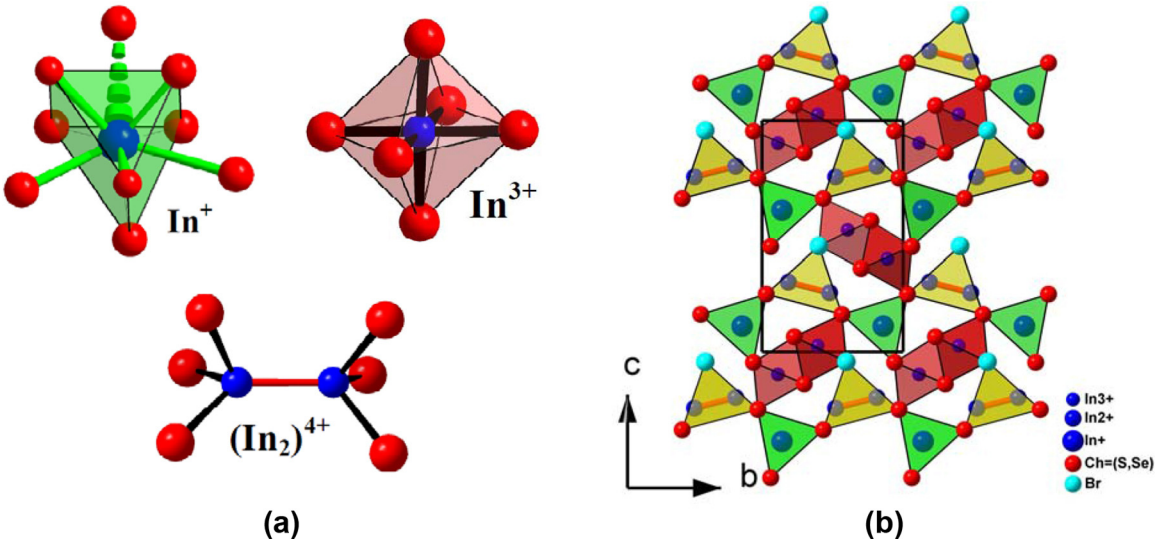

Fig. 4. (a) Indium coordinations in the ternary compound In_5Se_5Br: three capped prismaticcoordination of In^+; ethane analogue units built by two In^{+2} covalently bonded and six chalcogen atoms; octahedral coordination of In^{+3}, (b) projection of the In_5Se_5B structure along (1 0 0) where each double octahedra is surrounded by six triangles.

lengths of a few millimeters and diameters varying from 5–30 μm (Fig. 3a). The qualitative elemental analysis based on EDX measurements for the dark-brownish needle-shaped crystals of In_5Se_5Br revealed the presence of the respective elements. Due to the small difference in the number of electrons between Se and Br, an overlapping of the Br-L line and the Se-L line occurs (Fig. 3b).

3.2. Structure *and structural characteristics of In_5Se_5Br*

The compound In_5Se_5Br crystallizes in the orthorhombic crystal system, with the space group $Pmn2_1$ and lattice constants $a = 4.0932(3)$ Å, $b = 9.3331(7)$ Å, $c = 15.251(2)$ Å, $V = 582.60(8)$ Å^3 [50]. Based on the nomenclature proposed by Robin and Day [51], these compounds can be classified in the first group of mixed valence compounds where, indium occurs simultaneously in three different oxidation states: In^+, formal In^{2+} and In^{3+}. Meanwhile the selenium and bromine atoms possess their lowest oxidation numbers [Se^{2-}] and [Br^-].

The explicit formula of this compound can be written as follows: $In_5Se_5Br = [In^+]\ [(In_2)^{4+}]\ 2[In^{3+}]\ 5[Se^{2-}]\ [Br^-]$. In this structure In^+ is located in three capped trigonal prismatic holes; In^{2+} builds with its neighbored In^{2+} covalent bonded dumbbells $(In_2)^{4+}$, where each indium atom is further coordinated by three chalcogenides. In^{3+} is octahedrally coordinated.

Considering the projection along (1 0 0) the structure of In_5Se_5Br can be regarded as a mosaic where every edge sharing double octahedra is surrounded by six trigonal prisms (presented as triangles in the selected projection, Fig. 4). The stapling of these layers along (1 0 0) determines the length of the individual needle-shaped crystal.

3.3. Thermoelectric properties

The Seebeck voltage variation as a function of the temperature difference ranging from 0–80 K for bulk sample of In_5Se_5Br is represented by the plot of Fig. 5a. The ternary compound In_5Se_5Br displays a linear increase of the Seebeck voltage with the increasing temperature difference (Fig. 4a), representing though *n*-type semiconductor. A Seebeck voltage of up to 712 mV was recorded for the temperature difference of 80 K. This corresponds

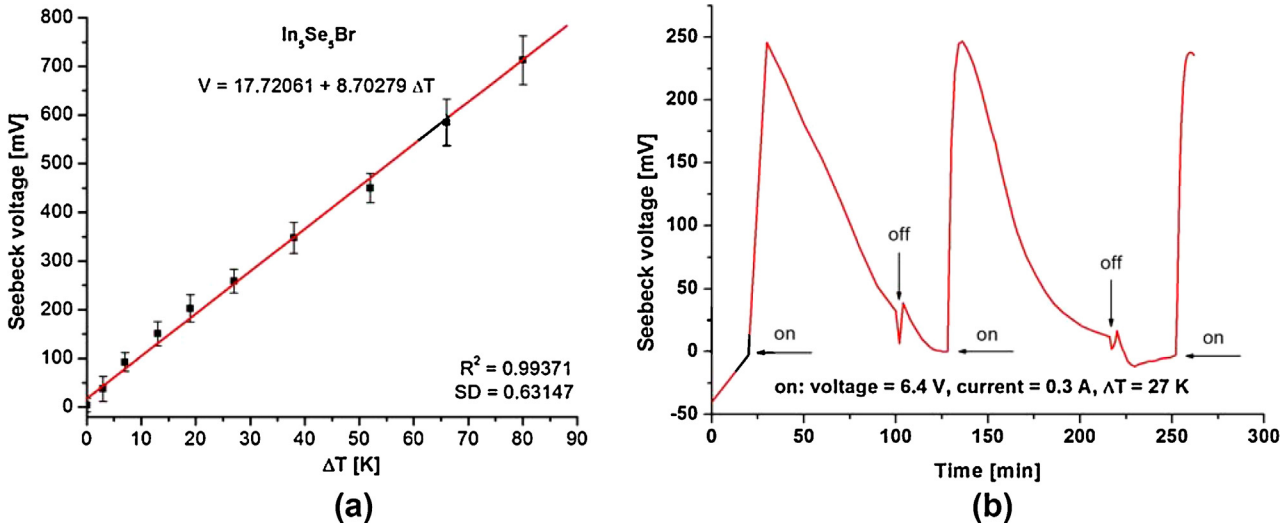

Fig. 5. (a) Variation of Seebeck voltage with the temperature difference for the mixed valence ternary compound In_5Se_5Br, (b) time-evolution of Seebeck voltage of the ternary compound In_5Se_5Br recorded for consequent switch on-off of the hot contact heating coil.

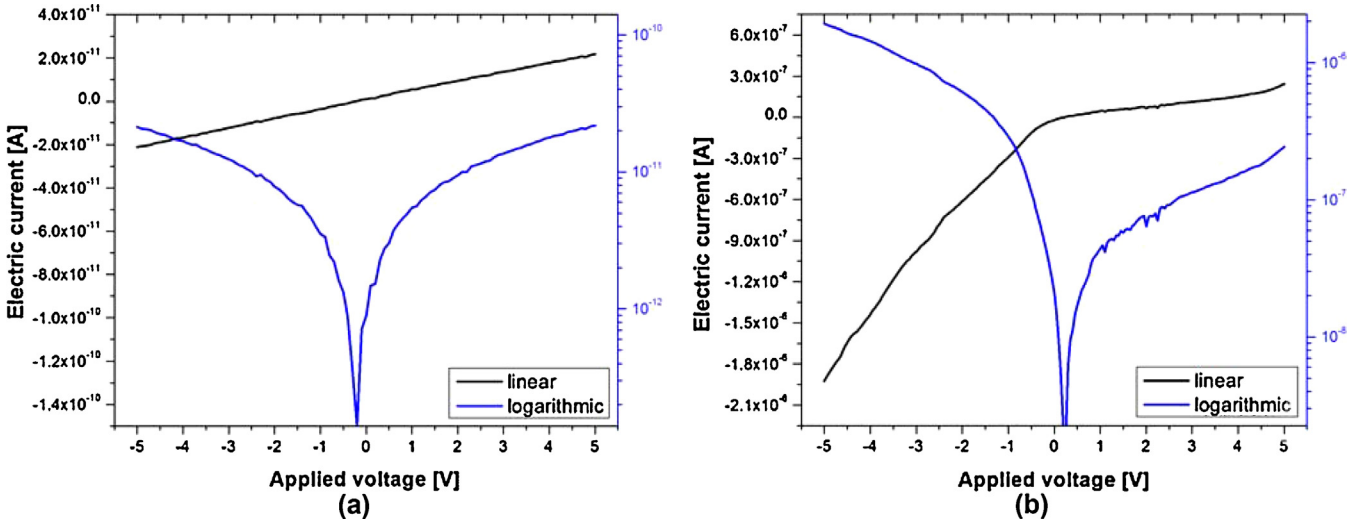

Fig. 6. *I–U* curves of In_5Se_5Br recorded from: (a) single crystal in absence of light (b) bulkcrystals.

to an extremely high Seebeck coefficient of −8900 μV/K. The slope of the linear fitting function indicates a mean Seebeck coefficient of −8702.79 μV/K

The time-evolution of the Seebeck voltage of bulk In_5Se_5Br exposed to a temperature difference between both sample contacts of 27 K (corresponding to power generator parameters: 6.4 V; 0.3 A) displayed a rapid increase up to approx. 250 mV (Fig. 5b). This value was stable just for a couple of seconds. Right after that, the Seebeck voltages decreased with a similar rate to the increasing one. This observation is related to the considerable thermal conductivity of the sample which is associated by continuous decreases of temperature difference in it. The Seebeck voltage approached zero once the temperature between both bulk sample contacts equals. The periodicity of this behavior as well as the repeatability of the Seebeck voltages upon consequent sample heating and cooling (power switch on-off) was observed.

3.4. Electric properties of bulk and single crystal In_5Se_5Br

The metal-semiconductor contact can either be an Ohmic contact or a Schottky barrier depending on the Fermi surface alignment and the nature of the interface between the metal and the semiconducting micro-wire. Usually, in heavy doped semiconductors both contacts are considered ohmic contacts leading so far to linear shaped *I–U* behaviors. This is the case of the single crystal of In_5Se_5Br (Fig. 6a) unlike the bulk sample of In_5Se_5Br which shows a rectifying *I–U* characteristic (Fig. 6b). According to Zhang et al. [52] this happens when one metal-semiconductor is an ohmic contact while the other remains a Schottky contact. Meanwhile in such bulk sample, depending on the random orientation of the microwires one cannot exclude the differences between the conductivities of the microwires in each crystallographic direction, the charge transport at the interfaces etc.

The plot expressing the applied voltage vs. the electric current for a single crystal of In_5Se_5Br results to a straight line (Fig. 7a), the slope of which is directly related to the electrical resistivity of the microwire based on the Eq. (1)

$$R = \frac{dU}{dI} \tag{1}$$

Based on this equation the resistivity of the measured single crystal of In_5Se_5Br results $2.32 \times 10^{11}\ \Omega$. Considering a microwire

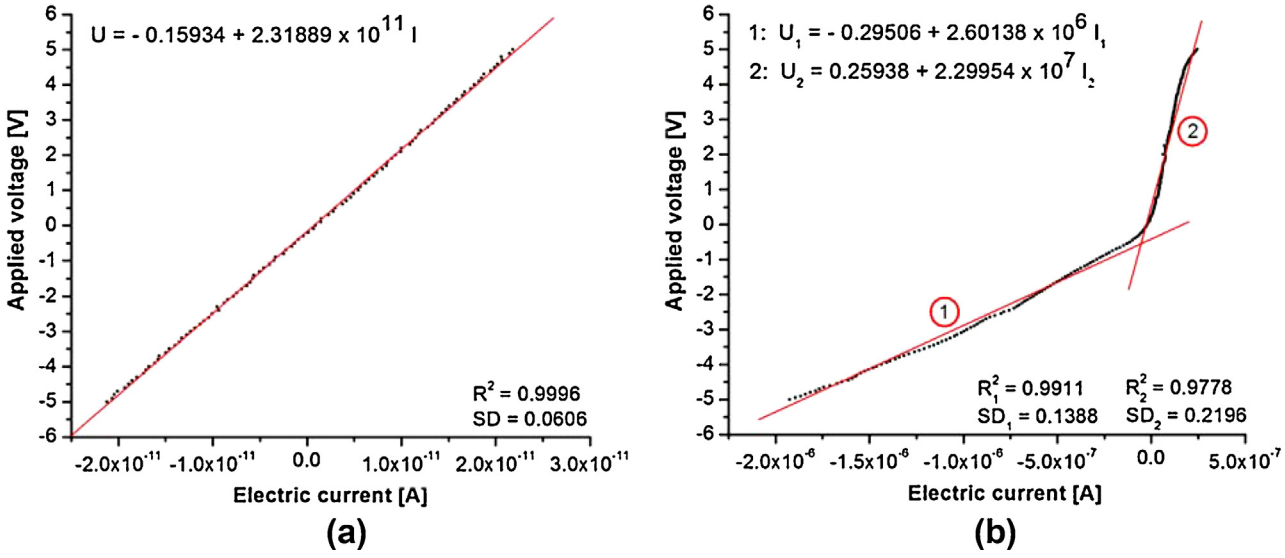

Fig. 7. Experimental (dots) and fitted U vs. I (red-lines) plot for In_5Se_5Br corresponding to (a) a single crystal, (b) a bulk sample. (For interpretation of the references to colour in this figure legend, the reader is referred to the web version of this article.)

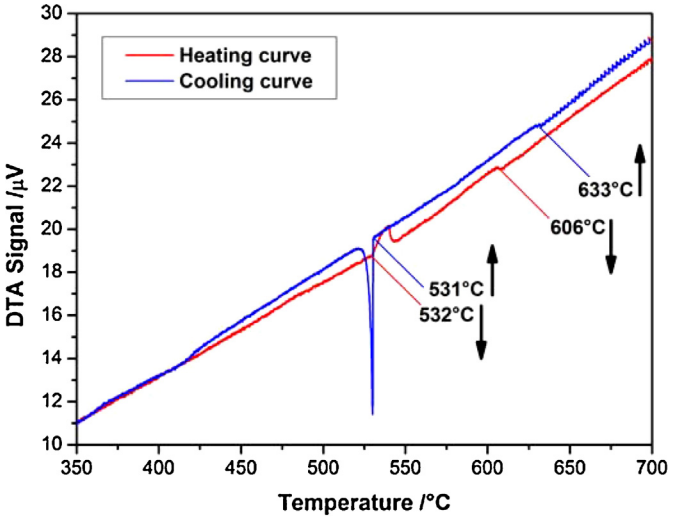

Fig. 8. Section of the DTA-curve of In_5Se_5Br. The heating curve plotted in red shows an endothermic effect at 532 °C (805 K) followed by a broad and less intensive one at 606 °C (879 K). The cooling curve depicted in blue, shows a dingy exothermic effectat 633 °C (906 K) followed by an intensive one at 53 °C (805 K). The up and down arrows (⇅) represent the exothermic and endothermic effects, respectively. (For interpretation of the references to colour in this figure legend, the reader is referred to the web version of this article.)

with a length of 2 mm and a cross-section of approx. 78.5 μm^2 this would yield a specific electrical resistivity of 9.1 kΩ. Bulk sample of crystalline In_5Se_5Br shows a lower electrical resistance for negative applied voltages followed a higher electrical resistivity for positive voltages. This turns the resistivity's calculation of bulk In_5Se_5Br more complex. The *U–I* plot of bulk In_5Se_5Br can be considered as built of two discrete straight lines due to its inflection near 0 A (Fig. 7b), representing each an electrical resistivity of 2.6 MΩ and 23 MΩ respectively, and a mean resistivity of approx. 13 MΩ.

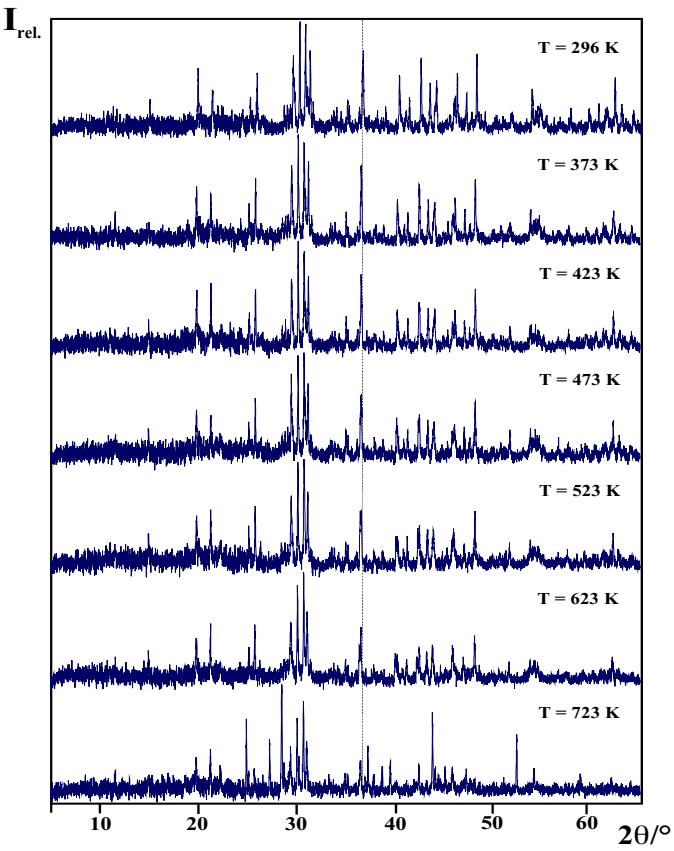

Fig. 9. Powder diffraction patterns of In_5Se_5Br measured at different temperatures. The dashedline reveals the displacement of the chosen reflection to lower 2θ – values with temperature increase.

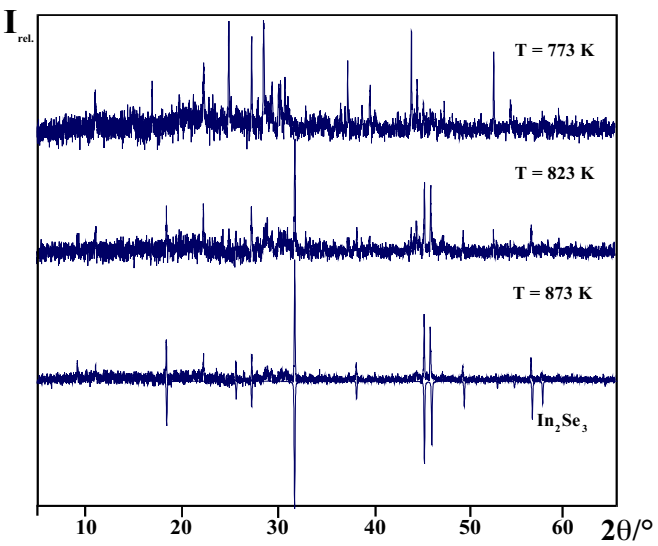

Fig. 10. The stepwise decomposition of In_5Se_5Br starting approximately at 723 K. Comparison of the powder pattern recorded at high temperatures with the calculated diffraction pattern of In_2Se_3.

3.5. Thermal behavior

The mixed valence crystalline compound In_5Se_5Br is stable in air. Its thermal behavior investigated by DTA (Fig. 8) shows several effects. The heating curve plotted in red shows an endothermic effect(↓) at 532 °C (805 K) followed by an increased background (broad and less intensive endothermic effect) which ends at 606 °C (879 K). The cooling curve depicted in blue, shows a dingy exothermic effect(↑) at 633 °C (906 K) followed by another intensive one at 532 °C (805 K).

Based on these data it is assumed that In_5Se_5Br decomposes at 532 °C (805 K) merely to the binary compounds: InBr (285 °C; 558 K), InSe (618 °C; 891 K) and In_2Se_3 (890 °C; 1163 K). As observed by the respective melting/transforming temperatures of these binary compounds, only InBr transforms immediately to the amorphous phase, InSe approaches its peritectic melting around 606 °C ± 10 °C while In_2Se_3 remains still as a solid. The depicted heating and cooling curves (Fig. 8) reveal that the thermal process of In_5Se_5Br is partially reversible. The exothermic process at 633 °C observed at the cooling curve (Fig. 8) belongs probably to the formation/solidification of In_xSe_y (x = 4, 5; y = 3, 6), meanwhile further cooling leads to partial formation/solidification of In_5Se_5Br (531 °C; 804 K) along with other binary by-compounds as confirmed by post DTA powder XRD measurements.

For a detailed investigation of its thermal stability along with its thermal expansion and thermal decomposition mechanism a series of high-temperature powder XRD measurements were performed. The HT-powder XRD measurements proceeded measuring in region 5–65° (2θ), measuring step 0.1° and a ratio time/step 120 s, ω-rotation = 2.5. The studied temperature range was within the interval 296–873 K. The recorded powder patterns are exhibited in Figs. 9 and 10 . The indexation of the reflections and the refinement of the lattice parameters in the space group $Pmn2_1$ succeeded until 723 K. At higher temperatures the measured powder patterns show difficulties in the indexing of the reflections

Table 1
Lattice parameters of In_5Se_5Br obtained at different temperatures

T/K	a/Å	b/Å	c/Å	V/Å^3
296(4)	4.099(1)	9.336(2)	15.250(4)	583.6(2)
373(4)	4.1037(7)	9.3569(9)	15.251(2)	585.6(1)
423(4)	4.1056(8)	9.3607(9)	15.255(2)	586.3(1)
473(4)	4.1089(7)	9.375(1)	15.257(2)	587.7(1)
523(4)	4.115(1)	9.386(1)	15.255(4)	589.1(2)
623(4)	4.120(1)	9.403(1)	15.262(3)	591.3(2)
723(4)	4.1232(8)	9.431(2)	15.275(2)	594.0(1)

due to the presence of the decomposition products associated by the decrease of the reflections intensities. Their dependence as a function of temperature is presented graphically in Figs. 9 and 10. The lattice constants determined from these powder patterns measured at different temperatures are listed in Table 1.

A close observation of the powder patterns of In_5Se_5Br recorded within the temperature interval 723–773 K reveals some extra reflections which are absent in the bordering powder patterns recorded at 623 K and 823 K. In order to characterize this "new phase" present in both diffraction patterns, a careful manual reflection (line) selection was performed in both cases. The indexation of these lines based on Louer's algorithm revealed in each case a "new" orthorhombic phase along with the existing one. The obtained lattice parameters from these indexations and consequent refinements are listed in Table 2 along with the lattice parameters of In_5Se_5Br at 733 K for comparison reason.

As observed from Table 2, both orthorhombic phases differ considerably.

The combination of the above DTA data with the information obtained by the X-ray powder patterns recorded at increasing temperatures emphasises the fact that In_5Se_5Br decomposes partially at 532 °C (805 K) yielding as the decomposition products the binary compounds: InBr and orthorhombic In_xSe_y. The first compound having a lower melting points than In_5Se_5Br undergoes the transformation solid–liquid at the decomposition temperature, meanwhile, In_xSe_y ($x = 4, 5$; $y = 3, 6$) transforms further to InSe and In_2Se_3 (m.p. 1163 K) which remains crystalline at this temperature, as shown by the remaining reflections above 805 K. Furthermore, to better elucidate the thermal behavior of In_5Se_5Br, the thermal expansion coefficients are calculated based the respective lattice parameters listed in Table 3.

The presence of structural blocks oriented along (0 1 0) direction (Fig. 4b) with the highest atomic density exhibits the highest elongation along b axis with 1.02% corresponding to a coefficient of thermal expansion in b direction of $\alpha_b = 2.3(4) \times 10^{-5}$ K^{-1} (determined until 723 K). Meanwhile due to the looser confinement along a and c directions their elongation is merely 0.6% and 0.16% corresponding to mean coefficients of thermal expansion of $\overline{\alpha_a} = 1.3(1) \times 10^{-5}$ K^{-1}, $\overline{\alpha_c} = 4.4(5) \times 10^{-6}$ K^{-1} respectively. The coefficient of the volume expansion is $\alpha_V = 4.2(4) \times 10^{-5}$ K^{-1}.

3.6. Perspective research and outlook

On one hand the large Seebeck coefficient (S) observable in In_5Se_5Br is a result of a combination of sufficient density of charge carriers and small Fermi energy. On the other hand, the presence of relatively heavy atoms such as In, Se and Br in In_5Se_5Br attributes it low lattice thermal conductivity. Despite of these promising parameters, in order to have a high thermoelectric efficiency expressed by the dimensionless figure of merit $ZT = \sigma S^2 T/\kappa$ (σ = electrical conductivity, S = Seebeck coefficient, T = absolute temperature, κ = thermal conductivity) one should increase the electrical conductivity and the Seebeck coefficient and consequently reduce the thermal conductivity. For In_5Se_5Br the last two mentioned parameters are very promising, unlike the electrical conductivity which is lower than expected (43 nS).

The improvement of ZT for this compound makes our near-future challenge. To achieve this goal we have sought two simultaneous strategies:

(a) Synthesis of thin films of In_5Se_5Br on glass substrates, containing nanowires deposited onto the surface through strict controlling of parcial pressures of the starting binary compounds. On one hand, the preferential one-direction crystal growth, referred as reduced dimensionality is often combined to unusual atomic arrangements which constrain the charge carriers in crystals to move preferentially in one direction. The low-dimensional configurations represented by superlattices and quantum well structures in nano- and micro-wires have exhibited enhanced thermoelectrics performance due to the lowering of phonon barrier at corresponding interfaces [53,54]. Venkatasubramanian et al. elaborated these strategy in the structures of Bi_2Te_3/Sb_2Te_3 creating superlattices with a period of 6 nm which yielded a figure of merit $ZT > 2$ [55,56].

(b) Growing thin films of In_5Se_5Br nano-crystals on glass substrate solicitates the Na intercalation which combined with targeted substitution and doping strategies can show significant influence on the density of the carrier concentration. Sometimes such a point defect scattering in a compound are associated with a decrease of the lattice thermal conductivity further compared to the compound having no point defect. Ahn et al. [57] showed that the substitution of an indium site with Na, Ca and Pb showed higher electron concentration than other substituting atoms. The process of doping or substitution for the improvement of the thermoelectric properties was successfully employed in clathrates [33,58–59] and Heuslers [35] where decreased resistivities, lower thermal conductivities and higher ZT values were observed.

Table 2
Lattice parameters of In_5Se_5Br at 723 K and of the "new orthorhombic" phase observed at 723 K and 773 K (highlighted).

T/K	a/Å	b/Å	c/Å	V/Å^3
723(4)	4.1232(8)	9.431(2)	15.250(2)	594.0(1)
723(4)	19.589(14)	9.3569(9)	6.183(3)	432.3(4)
773(3)	19.606(11)	9.3607(9)	6.185(2)	432.9(3)

Table 3
The coefficients of the thermal expansion α_a and α_c (In_5Se_5Br) calculated at different temperatures.

T/K	α_a x 10^{-5}/K^{-1}	α_c x 10^{-6}/K^{-1}
296(4)	0.7(1)	5.2(5)
373(4)	1.5(1)	2.8(5)
423(4)	1.7(1)	2.0(5)
473(4)	1.9(1)	1.9(5)
523(4)	1.8(1)	2.4(5)
623(4)	1.3(1)	5.4(5)
723(4)	0.2(1)	11.0(5)

4. Conclusions

We reported on the ternary mixed valence inorganic solid, In_5Se_5Br which consists of needle-shaped crystals crystallizing in the space group $Pmn2_1$. It exhibits unusually high Seebeck voltage measured in bulk and behaves as n-type semiconductor showing linear proportionality of the Seebeck voltage toward temperature

difference. On one hand, a Seebeck voltage of up to 712 mV was recorded for the temperature difference of 80 K, corresponding to unusually high Seebeck coefficient of $-8900\,\mu V/K$. The bulk sample Seebeck voltage was reproducible and sensitive toward the sample temperature gradient. On the other hand, the *I–U* curve of a single crystal showed ohmic characteristics (linear behavior) and a resistivity of $2.32 \times 10^{11}\,\Omega$. Bulk sample in contrast displayed an *I–U* rectifying curve associated by a moderated mean resistivity of 13 MΩ. In_5Se_5Br was stable in air and partially decomposes at 805 K to InBr and In_xSe_y ($x = 4, 5$; $y = 3, 6$). The latter orthorhombic phase transforms further to InSe and In_2Se_3. Within 723 K and 773 K a "new orthorhombic" phase coexisting with the primary phase is observed. The indexation and the refinement of powder patterns succeeded up to 723 K revealing *b* axis with the highest elongation of 1.02% and mean coefficient of thermal expansion $\alpha_b = 2.3(4) \times 10^{-5}\,K^{-1}$. The elongations of *a* and *c* axes were merely 0.6% and 0.16% corresponding to mean coefficients of thermal expansion of $\overline{\alpha_a} = 1.3(1) \times 10^{-5}\,K^{-1}$, $\overline{\alpha_c} = 4.4(5) \times 10^{-6}\,K^{-1}$, respectively. Two strategies related to the way of synthesis combined with the controlled doping and targeted substitutions are sought to be implemented for the increase of the thermoelectric performance.

References

[1] C. Wood, Materials for thermoelectric energy conversion, Rep. Prog. Phys. 51 (4) (1988) 459–539.
[2] C.M. Bhandari, D.M. Rowe, Thermal Conduction in Semiconductors, Wiley Eastern Limited, New Delhi, India, 1988, pp. 224.
[3] I. Nishida, Study of semiconductor-to-metal transition in Mn-doped $FeSi_2$, Phys. Rev. B 7 (1973) 2710–2713.
[4] I. Nishida, T.J. Sakata, Semiconducting properties of pure and Mn-doped chromium disilicides, J. Phys. Chem. Solids 39 (1978) 499–505.
[5] T. Kojima, Semiconducting and thermoelectric properties of sintered iron disilicide, Phys. Status Solidi A 111 (1989) 233–242.
[6] J.C. Bass, N.B. Elsner, Segmented selenide thermoelectric generator, in: K.R. Rao (Ed.), Proceedings of the 3rd International Conference on Thermoelectric Energy Conversion, IEEE, Piscataway, New York, 1980, pp. 8–12.
[7] J.F. Nakahara, T. Takeshita, M.J. Tschetter, B.J. Beaudry, K.A. Gschneidner Jr., Thermoelectric properties of lanthanum sulfide with Sm, Eu, and Yb additives, J. Appl. Phys. 63 (1988) 2331–2336.
[8] C. Wood, D. Emin, Conduction mechanism in boron carbide, Phys. Rev. B 29 (1984) 4582–4587.
[9] S. Yugo, T. Sato, T. Kimura, Thermoelectric figure of merit of boron phosphide, Appl. Phys. Lett. 46 (1985) 842–844.
[10] N. Okinaka, T. Akiyama, Thermoelectric properties of nonstoichiometric TiO as a promising oxide material for high-temperature thermoelectric conversion, Proceedings of the 24th International Conference on Thermoelectrics (ICT 2005), IEEE, New York, 2005, pp. 34–37.
[11] P. Boudjouk, M.P. Remington Jr., D.G. Grier, Tris(benzylthiolato) bismuth. efficient precursor to phase pure polycrystalline Bi_2S_3, Inorg. Chem. 37 (14) (1998) 3538–3541.
[12] H.T. Shaban, M.M. Nassary, M.S. El-Sadek, Transport properties of Bi_2S_3 single crystals, Physica B 403 (2008) 1655–1659.
[13] T. Caillat, C.K. Huang, J.P. Fleurial, G.J. Snyder, A. Borshchevsky, Synthesis and thermoelectric properties of some materials with the $PbBi_4Te_7$ crystal structure, Proceedings of the XVII International Conference on Thermoelectrics, Cardiff, 2000, pp. 151–154.
[14] J. Jiang, L. Chen, S. Bai, Q. Yao, Q. Wang, Thermoelectric properties of *p*-type $(Bi_2Te_3)_x(Sb_2Te_3)_{1-x}$ crystals prepared via zone melting, J. Cryst. Growth 277 (2005) 258–263.
[15] H.W. Jeon, H.P. Ha, D.B. Hyun, J.D.J. Shim, Electrical and thermoelectrical properties of undoped Bi_2Te_3–Sb_2Te_3 and Bi_2Te_3–Sb_2Te_3–Sb_2Se_3 single crystals, J. Phys. Chem. Solids 52 (1991) 579–585.
[16] H.J. Goldsmid, Electronic Refrigeration, 1st ed., Pion Ltd, London, 1986.
[17] L.E. Shelimova, T.E. Svechnikova, P.P. Konstantinov, O.G. Karpinsky, E.S. Avilov, M.A. Kretova, V.S. Zemskov, Crystallographic constitution and the thermoelectric properties of mixed layered tetradymite-like ternary compounds, Proceedings of the 25th International Conference on Thermoelectrics (ICT06), Vienna, August, 2006, pp. 358–362.
[18] M.G. Kanadzidis, Semiconductors and Semimetals, Academic Press, San Diego, San Francisco, N.Y, 2001, pp. 50–98.
[19] L.E. Shelimova, P.P. Konstantinov, O.G. Karpinsky, E.S. Avilov, M.A. Kretova, V.S. Zemskov, VS, X-ray diffraction study and electrical and thermal transport properties of the $nGeTe \cdot mBi_2Te_3$ homologous series compounds, J. Alloy. Comp. 329 (12) (2001) 50–62.
[20] L.E. Shelimova, O.G. Karpinsky, P.P. Konstantinov, E.S. Avilov, M.A. Kretova, V.S. Zemskov, The *n*-and *p*-type mixed layered tetradymite like compounds with low. Lattice thermal conductivity: growth, structure and thermoelectric properties, Proceedings of the 6th European Workshop on Thermoelectrics, Freiburg, September, 2001, pp. 8–82.
[21] L.D. Ivanova, Y.V. Granatkina, Y.A. Sidorov, Electrical properties of antimony telluride crystals doped with selenium and bismuth, Inorg. Mater. 35 (1) (1999) 34–41.
[22] J.X. Zhang, Q.M. Lu, K.G. Liu, L. Zhang, M.L. Zhou, Synthesis and thermoelectric properties of $CoSb_3$ compounds by spark plasma sintering, Mater. Lett. 58 (14) (2004) 1981–1984.
[23] B.C. Sales, D. Mandrus, R.K. Williams, Filled skutterudite antimonides: a new class of thermoelectric materials, Science 272 (1996) 1325.
[24] B.X. Chen, J.H. Xu, C. Uher, D.T. Morelli, G.P. Meisner, J.P. Fleurial, T. Caillat, A. Borshchevsky, Low-temperature transport properties of the filled skutterudites $CeFe_{4-x}$ Co_x Sb_{12}s, Phys. Rev. B 55 (1997) 1476–1480.
[25] B.C. Sales, D. Mandrus, B.C. Chakoumakos, V. Keppens, J.R. Thompson, Electron crystals and phonon Filled skutterudite antimonides: glasses, Phys. Rev. B 56 (1997) 15081–15089.
[26] B.C. Sales, B.C. Chakoumakos, D. Mandrus, Thermoelectric troperties of thallium-filled skutterudites, Phys. Rev. B 61 (2000) 2475–2481.
[27] X.F. Tang, L.D. Chen, T. Goto, T. Hirai, Effects of Ce filling fraction and Fe content on the thermoelectric properties of Co-rich $Ce_yFe_xCo_{4-x}Sb_{12}$, J. Mater. Res. 16 (3) (2001) 837–843.
[28] D.T. Morelli, G.P. Meisner, Low temperature properties of the filled skutterudite $CeFe_4Sb_{12}$, J. Appl. Phys. 77 (1995) 3777–3782.
[29] G.S. Nolas, G.A. Slack, D.T. Morelli, T.M. Tritt, A.C. Ehrlich, The effect of rare earth filling on the lattice thermal conductivity of skutterudites, J. Appl. Phys. 79 (1995) 4002–4008.
[30] G. Nolas, J.L. Cohn, G. Slack, S.B. Schujman, Semiconducting ge clathrates: promising candidates for thermoelectric applications, Appl. Phys. Lett. 73 (1998) 178–180.
[31] M.M. Shatruk, K.A. Kovnir, A.V. Shevelkov, I.A. Presniakov, B.A. Popovkin, First tin pnictide halides $Sn_{24}P_{19.3}I_8$ and $Sn_{24}As_{19.3}I_8$: synthesis and the clathrate-I type of the crystal structure, Inorg. Chem. 8 (15) (1999) 3455–3457.
[32] K. Kishimoto, T. Koyanagi, K. Akai, M. Matsuura, Synthesis and thermoelectric properties of type-I clathrate compounds $Si_{(46-x)}P_xTe_8$, Jpn. J. Appl. Phys. Part 2 Lett. Exp. Lett. 32 (2007) 746–748.
[33] S.J. Kim, S. Hu, C. Uher, T. Hogan, B. Huang, J.D. Corbett, M.G. Kanatzidis, Structure and thermoelectric properties of Ba_6Ge_{25-x}, $Ba_6Ge_{23}Sn_2$, and $Ba_6Ge_{22}In_3$: zintl phases with a chiral clathrate structure, J. Solid State Chem. 153 (2000) 321–329.
[34] C. Uher, J. Yang, S. Hu, D.T. Morelli, G.P. Meisner, Transport properties of pure and doped MNiSn (M = Zr, Hf), Phys. Rev. B 59 (1999) 8615–8621.
[35] Y. Ono, S. Inayama, H. Adachi, Kajitani, T, Thermoelectric properties of doped half-Heuslers $NbCoSn_{1-x}Sb_x$ and $Nb_{0.99}Ti_{0.01}CoSn_{1-x}Sb_x$, Jpn. J. Appl. Phys. 45 (2006) 8740–8743.
[36] D.Y. Chung, T. Hogan, P. Brazis, M. Rocci-Lane, C. Kannewurf, M. Bastea, C. Uher, M. Kanatzidis, $CsBi_4Te_6$: a high-performance thermoelectric material for low-temperature applications, Science 287 (2000) 1024–1027.
[37] K.F. Hsu, S. Loo, F. Guo, W. Chen, J.S. Dyck, C. Uher, T. Hogan, E.K. Polychroniadis, M.G. Kanatzidis, Cubic $AgPb_mSbTe_{2+m}$: bulk thermoelectric materials with high figure of merit, Science 303 (2004) 818–821.
[38] E. Quarez, K.F. Hsu, R. Pcionek, N. Frangis, E.K. Polychroniadis, M.G. Kanatzidis, Nanostructuring, compositional fluctuations, and atomic ordering in the thermoelectric materials $AgPb_mSbTe_{2+m}$. The myth of solid solutions, J. Am. Chem. Soc. 127 (2014) 9177–9190.
[39] P.F.P. Poudeu, J. D'Angelo, A.D. Downey, J.L. Short, T.P. Hogan, M.G. Kanatzidis, High thermoelectric figure of merit and nanostructuring in bulk p-type $Na_{1x}Pb_mSb_yTe_{m+2}$, Angew. Chem. Int. Ed. 45 (2006) 3835–3839.
[40] H. Dittrich, A. Bieniok, U. Brendel, M. Grodzicki, D. Topa, Sulfosalts – a new class of compound semiconductors for photovoltaic applications, Thin Solid Films 515 (2007) 5745–5750.
[41] S. Derakhshan, A. Assoud, N.J. Taylor, H. Kleinke, Crystal and electronic structures and physical properties of two semiconductors: $Pb_4Sb_6Se_{13}$ and $Pb_6Sb_6Se_{17}$, Intermetallics 14 (2006) 198–207.
[42] M. Heuer, G. Wagner, T. Doering, K. Bente, G. Kryukova, Nanowire arrangements of PbS–Sb_2S_3-compounds, J. Cryst. Growth 267 (2004) 745–750.
[43] G.N. Kryukova, M. Heuer, G. Wagner, T. Doering, K. Bente, Synthetic $Cu_{0.507(5)}Pb_{8.73(9)}Sb_{8.15(8)}I_{1.6}S_{20.0(2)}$ nanowires, J. Solid State Chem. 178 (2005) 376–381.
[44] G. Kryukova, M. Heuer, T. Doering, K. Bente, Micro-and nanowires of iodine-containing $Cu_4Bi_2S_9$, J. Cryst. Growth 306 (2007) 212–216.
[45] T.F. Lomelino, G. Mozurkewich, Semiconducting band gaps of three lead-antimony sulfosalts, Am. Mineral. 74 (1989) 1285–1286.
[46] R. Kaden, Synthese Struktur und physikalische Eigenschaften komplexer Metallsulfide Kylindrit $FeSn_4Pb_3Sb_2S_{14}$ und Boulangerit $Pb_5Sb_4S_{11}$ PhD Thesis, University of Leipzig, 2009.
[47] J.W. Sharp, B.C. Sales, D.G. Mandrus, B.C. Chakoumakos, Thermoelectric properties of Tl_2SnTe_5 and Tl_2GeTe_5, Appl. Phys. Lett. 74 (25) (1999) 3794–3796.
[48] B. Chen, C. Uher, L. Iordanidis, M.G. Kanatzidis, Transport properties of Bi_2S_3 and the ternary bismuth sulfides $KBi_{6.33}S_{10}$ and $K_2Bi_8S_{13}$, Chem. Mater. 9 (1997) 1655–1658.
[49] S. Xiao-ya, W. Li, C. Li-dong, C. Xi-hong, Thermoelectric properties of $M_xMo_6Te_8$ (M = Ag, Cu), T. Nonferr. Metal Soc. 19 (2009) 642–645.
[50] K. Xhaxhiu, The Use of Supercritical Carbon Dioxide in Solid State Chemistry and Basic Structural Investigations with Chalcogenide Halides of the Third Main Group. PhD Thesis, University of Siegen, 2005.

[51] M.B. Robin, P. Day, Mixed valence chemistry. A survey and classification, Adv. Inorg. Chem. Radiochem. 10 (1967) 247–422.
[52] Z.Y. Zhang, H. Jin, X.L. Liang, Q. Chen, L.-M. Peng, Current–voltage characteristics and parameter retrieval of semiconducting nanowires, Appl. Phys. Lett. 88 (1–3) (2006) 73102.
[53] L.D. Hicks, T.C. Harman, M.S. Dresselhaus, Use of quantum-well superlattices to obtain a high figure of merit from nonconventional thermoelectric materials, Appl. Phys. Lett. 63 (23) (1993) 3230–3232.
[54] N. Peranio, Structural, Chemical, and Thermoelectric Properties of Bi2te3 Peltier Materials: Bulk, Thin Films, and Superlattices PhD Thesis, Eberhard-Karls University of Tübingen, 2008.
[55] R. Venkatasubramanian, T. Colpitts, B. O'Quinn, S. Liu, N. El-Masry, M. Lamvik, Low-temperature organometallic epitaxy and its application to superlattice structures in thermoelectrics, Appl. Phys. Lett. 75 (1999) 1104–1106.
[56] R. Venkatasubramanian, Lattice thermal conductivity reduction and phonon localizationlike behavior in superlattice structures, Phys. Rev. B 61 (2000) 3091–3097.
[57] K. Ahn, E. Cho, J.-S. Rhyee, S.I. Kim, S.M. Lee, K.H. Lee, Effect of cationic substitution on the thermoelectric properties of $In_{4-x}M_xSe_{2.95}$ compounds (M = Na, Ca, Zn, Ga, Sn, Pb; x = 0. 1), Appl. Phys. Lett. 99 (1–3) (2011) 102110.
[58] K. Hayashi, T. Nozaki, T. Kajitani, Structure and high temperature thermoelectric properties of delafossite-type oxide $CuFe_{1-x}Ni_xO_2$ ($0 \leq \times \leq 0.05$), Japn. J. Appl. Phys. 46 (8A) (2007) 5226–5229.
[59] D.Y. Chung, A. Mrotzek, T. Kyratsi, T. Hogan, M.G. Kanatzidis, $CsMBi_3Te_6$ and $CsM_2Bi_3Te_7$ (M = Pb,Sn): new thermoelectric compounds with low-dimensional structures, J. Am. Chem. Soc. 124 (11) (2002) 2410–2411.